

A Simple and Fast Electrochemical CO₂ Sensor Based on Li₇La₃Zr₂O₁₂ for Environmental Monitoring

Michal Struzik, Inigo Garbayo, Reto Pfenninger, and Jennifer L. M. Rupp*

In the goal of a sustainable energy future, either the energy efficiency of renewable energy sources is increased, day-to-day energy consumption by smart electronic feedback loops is managed in a more efficient way, or contribution to atmospheric CO₂ is reduced. By defining a next generation of fast-response electrochemical CO₂ sensors and materials, one can contribute to local monitoring of CO₂ flows from industrial plants and processes, for energy management and building control or to track climate alterations. Electrochemical Li⁺-garnet-based sensors with Li₇La₃Zr₂O₁₂ solid electrolytes can reach notable 1 min response time at lowered operation temperatures to track 400–4000 ppm levels of CO₂ when compared with state-of-the-art NASICON-based sensors. By using principles of redefining the electrode electrochemistry, it is demonstrated that Li_{6.75}La₃Zr_{1.75}Ta_{0.25}O₁₂ can be used to alter its classic use as energy-storage function to gain additional functions such as CO₂ tracking.

Within the last 20 years the anthropogenic emission of greenhouse gasses has been doubled with 80% contribution of carbon dioxide.^[1] The U.S. National Oceanic and Atmospheric Administration South Pole climate monitoring station has reported carbon dioxide concentration over 400 ppm, approaching the level, where climate changes might be irreversible.^[2–5] That promotes development of long-term international strategy and collaboration on the limitation of greenhouse gasses emissions, and directs research attention onto their detection and capture methods.^[6] In addition to planet-wide monitoring, held by national agencies and global organizations, new possibilities

arise to monitor local CO₂ concentration in order to improve energy efficiency and feedback loops on exhausts as data through small sensing devices. Gas sensors integrated as control units into buildings infrastructure, vehicles, smartphones, and wearable devices contribute to real-time georeferenced chemical tracking, working as well as the feedback units to educate consumers and industry. That would allow not only to monitor large-scale industrial CO₂ emission from power generation, food production, or packaging industries,^[7] but also emission from nonindustrial buildings in order to improve energy efficiency of households and commercial areas. CO₂ monitoring is also essential for air-quality control of confined spaces such as office/laboratory areas or marine vessels, where increased carbon dioxide concentration

may not only influence laborers' well-being but also serves to assure their safety. Moreover, CO₂ tracking plays a major role in medical diagnosis for respiratory diseases and sleep disorder.^[8,9]

Nowadays popular CO₂ tracking devices are based on Fourier-transform infrared spectroscopy, showing very good accuracy (± 30 ppm of CO₂, $\pm 2\%$), selectivity, and fast response times (< 20 s).^[10] The nondispersive infrared CO₂ tracking devices are, however, limited by a narrow temperature operation window (0–50 °C), power consumption of around 40 mW for devices being operated in a pulsing mode rather than continuous and also show rather limited potential for further miniaturization due to optical configuration.^[11,12] A promising alternative to those rather expensive devices lies in electrochemical potentiometric CO₂ sensors.

In general, an electrochemical potentiometric gas sensor has a simple structure of an electrochemical cell, consisting of three functional components, namely, a sensing electrode, a solid-state electrolyte, and a reference electrode (RE). In such an arrangement, it is the selectivity of the electrode materials, which are used to detect gaseous species that is defining an electromotive force (EMF) of the cell, measured as a cell potential. Potential, as an intrinsic property, is independent on geometry or mass changes of the device, offering high scalability potential for future miniaturization. Here, the EMF manifested as voltage through the cell is related to the relative partial pressure of detected specimen at the electrodes as postulated by the Nernst equation.^[13] Depending on the relation between gas and mobile specimen in the solid electrolyte, three types of potentiometric gas sensors can be distinguished, according to Weppner's classification^[14] (Figure 1).

Dr. M. Struzik, R. Pfenninger, Prof. J. L. M. Rupp
Electrochemical Materials
Department of Material Sciences and Engineering
Massachusetts Institute of Technology
77 Massachusetts Avenue, Cambridge, MA 02139, USA
E-mail: jrupp@mit.edu

Dr. M. Struzik, Dr. I. Garbayo, R. Pfenninger, Prof. J. L. M. Rupp
Electrochemical Materials
ETH Zurich
Department of Materials
Hoengerbergring 64, 8049 Zurich, Switzerland
Prof. J. L. M. Rupp
Electrochemical Materials
Department of Electrical Engineering and Computer Science
Massachusetts Institute of Technology
77 Massachusetts Avenue, Cambridge, MA 02139, USA

 The ORCID identification number(s) for the author(s) of this article can be found under <https://doi.org/10.1002/adma.201804098>.

DOI: 10.1002/adma.201804098

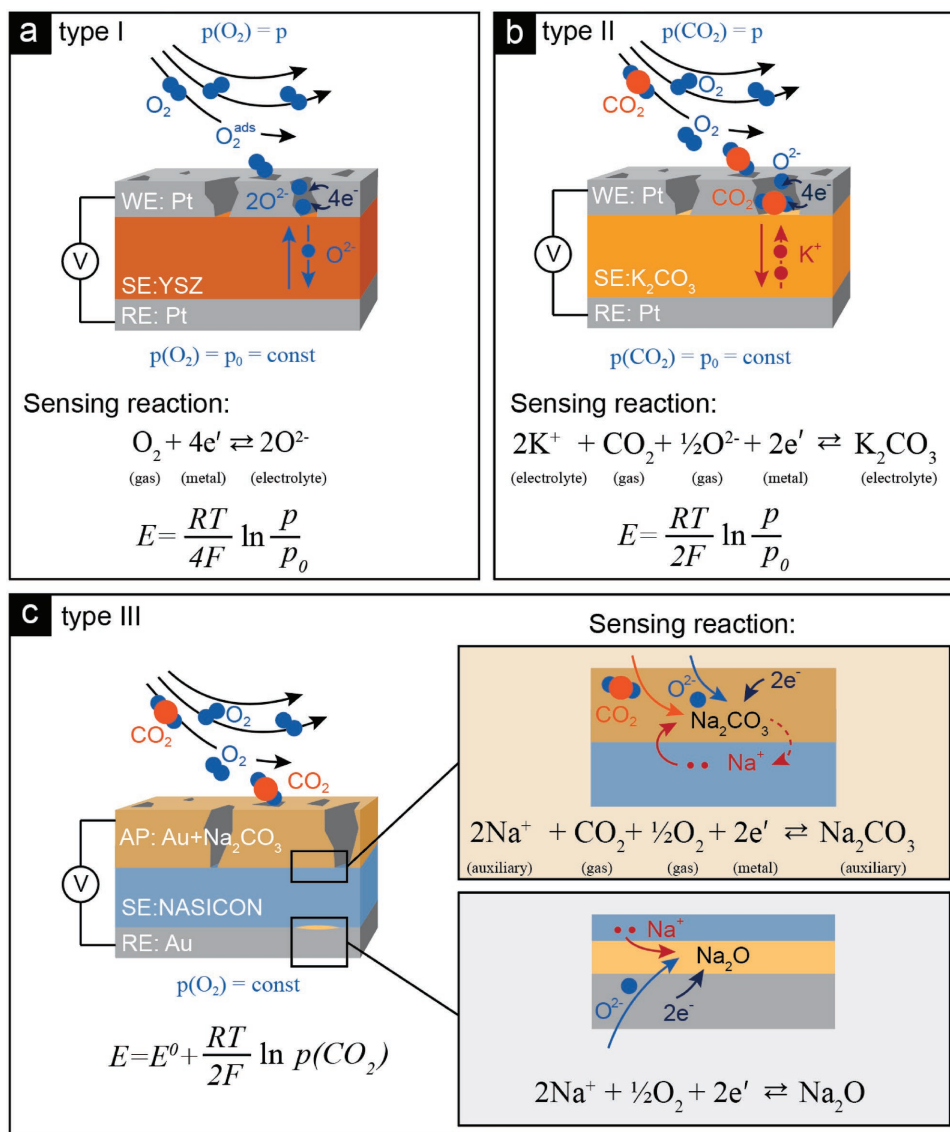


Figure 1. Sensing principle of potentiometric gas sensors. a) Type I gas sensor for O_2 detection, using a thin layer of Pt as the reference (RE) WE and yttrium-stabilized zirconia (YSZ) as the solid electrolyte (SE), b) type II gas sensor for CO_2 detection using K_2CO_3 as a solid electrolyte, and c) type III gas sensor for CO_2 detection NASICON-based solid electrolyte, Na_2CO_3 auxiliary phase (AP) utilized as sensing electrode and Pt RE.

In the *type I* gas sensor, the detected species is converted into the mobile species in the electrolyte; to exemplify, the O_2 sensor is shown in Figure 1a. The sensing reaction occurs at the triple phase boundary (TPB), where an oxygen conducting solid-state electrolyte, such as yttria-stabilized zirconia (YSZ), sensing electrode material, i.e., porous Pt, and the gaseous phase containing oxygen are in contact with each other. At the TPB, oxygen molecule gets adsorbed on the surface of Pt and converted to O^{2-} ions, which further diffuse into the electrolyte.^[15,16] The surface reaction changes the chemical potential of the sensing electrode, which implies change of the EMF of the cell, defined in the Nernst equation by a difference of chemical potentials between the sensing and REs, and is measured as a cell voltage. The *type II* gas sensor allows detecting specimen, which are identical to an immobile species in the electrolyte through a reaction with a second mobile ions.

As an example, the CO_2 sensor proposed by Gauthier is given, which utilizes K_2CO_3 as the solid electrolyte, where K^+ cations are the mobile ions^[17] (Figure 1b). Once adsorbed at the TPB, carbon dioxide molecules react with K^+ ions from the electrolyte, forming immobile K_2CO_3 , establishing new chemical potential on the sensing electrode and resulting in a changed EMF of the cell. Also, *type II* gas sensors can be used for NO_x and SO_x detection,^[18,19] however, the number of chemically stable combinations for solid electrolyte and sensing electrode materials are limited toward other gasses, being the major drawback of this sensor principle.^[20] *Type I* and *type II* sensors are usually two-chamber systems, where the chemical potential of the RE is fixed by a physical separation from the measurement chamber filled with detected specimen. The list of reported *type I* and *type II* sensing devices is, however, short, due to lack of suitable solid electrolytes conducting more complex species

such as NO_x, SO_x, or CO₂ for *type I* devices; similar limitations exist for *type II* devices, as only few electrolyte material exhibits required thermal and chemical stability and can be integrated in working environment due to gas tightness issues and reactivity with surrounding construction materials. In *type III* gas sensors an auxiliary phase is employed between the solid electrolyte and the sensing electrode or may also directly work as sensing electrode itself, simplifying the cell design (Figure 1c). The auxiliary phase contains both the detected species from the gaseous phase and the mobile carriers of the solid electrolyte such as sodium or lithium. With *type III* gas sensors comes a plethora of new materials and flexibility for materials combinations that can be used as the auxiliary phase and the solid electrolyte, which in turn opens perspectives for yet unexplored device designs, fabrication routes, and increased scalability. With this, new opportunities are emerging for lowered operation temperature, improved long-term stability, and reduced production costs. The choice of the solid electrolyte material is, however, nontrivial, as for its interfaces toward the electrodes a high ionic exchange rate is needed to assure a fast sensor response. In addition, long-term chemical stability over wide temperature and CO₂ concentration range requires not only high ionic conductivity but also ionic transference number $t_i = 1$ in order to prevent electronic leakage and related side processes, often leading to the sensitivity degradation. *Type III* sensors utilizing as electrolytes sodium-ionic conductors, commonly known as NASICON, have shown fast response times in a range of 60 s but suffer from high power consumption due to the required operating temperature above 400 °C.^[21–23] Operation of NASICON-based devices below 400 °C results in significant increase of the response time to more than 200s.^[23–25] A cause should be seen in high interfacial resistance between the auxiliary phase and electrolyte, as well as the slow gas kinetics on the auxiliary phase, which remains one of the most important challenges for energy efficient electrochemical devices. In addition, NASICON-based devices show stability issues, i.e., chemical instability against materials used as the auxiliary phase^[26–30] toward humidity^[31–34] and are prone to show cross-sensitivity toward other gasses.^[35] One strategy to overcome those challenges is the substitution of NASICON electrolytes with other available lithium-conducting electrolytes due to increased Li-reactivity toward CO₂, fast Li⁺ conduction, and the generally higher stability to moisture amongst other alkali metals.^[36] We review and compare state-of-the-art Li-solid state conductors (Li₃PO₄, LISICON, LiPON) to classic Na-conductors (i.e., NASICON) in their CO₂ sensing performance when employed as electrolytes for *type III* sensors (Table 1).

A number of *type III* CO₂ sensing devices using as a solid electrolyte Li₃PO₄,^[37–42] LiPON,^[43,44] or LISICON^[45] have been discussed for different cell configurations and auxiliary phases showing good sensitivity up to 5000 ppm of CO₂ and acceptably fast response time of 60 s at relatively high operation temperatures above 400 °C. On one side, high operation temperature is beneficial for the sensing reaction kinetics, as well as improved Li⁺ mobility in the TPBs and interfacial region between solid electrolyte and the electrodes, but also results in increased power consumption and may affect long-term stability of the device, due to possible deterioration processes of the cell

components and may obstruct cell integration with control electronic circuits. In essence, poor ionic mobility of rather slow ionic conductors, such as Li₃PO₄ (7×10^{-8} S cm⁻¹ at 25 °C),^[46,47] LiPON (2.3×10^{-6} S cm⁻¹ at 25 °C),^[43] or LISICON (10^{-5} S cm⁻¹ at 25 °C)^[48] might be dictating high operation temperature.

One of the strategies to improve electrochemical sensors' attractiveness for applications in terms of low power consumption and fast response time would be to promote higher Li⁺ mobility at TPBs and between the solid electrolyte and the auxiliary phase. There have been successful attempts of using very fast ceramic Li-conductors, such as Li_{3-x}La_{((2/3)-x)}((1/3)-2x)TiO₃ (1×10^{-3} S cm⁻¹)^[49,50] for CO₂ tracking.^[51] Lithium lanthanum titanate based devices show however phase stability issues due to reduction of Ti. Also materials with a garnet structure of general formula of Li₅La₃M₂O₁₂ (M = Ta⁵⁺, Nb⁵⁺) attract much attention due to their high and predominantly ionic conductivity in a range of 10^{-7} – 10^{-5} S cm⁻¹, which together with high tolerance for doping with aliovalent cations allows to tune their crystal phase and transport properties.^[52] Out of this family of compounds, Li₆BaLa₂Ta₂O₁₂ was recently employed as solid electrolyte with an Au–Li_{0.36}WO₃ RE and Li₂CO₃–Au auxiliary phase for CO₂ sensing device.^[53] The sensing performance was stable for a period of several days, showing close to theoretical sensitivity between 300 and 500 °C and response times below 1 min at 500 °C, being comparable with other CO₂ sensor *type III* cells based on Li-conductors of LiPON or LISICON. Long-term stability under real-life conditions such as under humid atmospheres remained however undiscussed.

In summary, potentiometric CO₂ sensors with lithium-conducting solid electrolytes are showing sensitivity to carbon dioxide in a range of 400–4000 ppm and rather high operation temperatures above 400 °C, similar to their sodium conductor based counterparts, but at the advantage of being less prone to humidity. High lithium mobility in the TPB plays a key role for lowering the sensor operation temperature and assuring fast kinetics of the sensing reaction with the gaseous species in the auxiliary phase, resulting in fast response times and improved devices' energy efficiency. Concluding, the utilized solid electrolyte material plays a major role in designing a stable CO₂ sensing architecture; for that we define that the high ionic exchange rates between the electrolyte and the electrodes are essential, as well as a chemical and thermal stability of all the sensing cell components. The additional contribution of the electronic conductivity in total conductivity of the electrolyte would lead to a side reaction, resulting in faster degradation of the device.

As a new aspect we propose to use Li₇La₃Zr₂O₁₂ in its cubic phase (c-LLZO) as a solid electrolyte for potentiometric *type III* CO₂ gas sensor. Recently, lithium lanthanum zirconate was successfully utilized as the electrolyte in ceramic solid-state batteries,^[54–57] due to its high ionic conductivity of 1.03×10^{-3} S cm⁻¹ at room temperature^[52,58–60] and negligible electronic conductivity.^[61] One of the major challenges for using Li-garnets in solid-state batteries is that Li₇La₃Zr₂O₁₂ exhibit stability challenges, when exposed to CO₂ and H₂O rich atmospheres resulting in high-resistive interfaces through formation of Li₂CO₃ in contact with air.^[62] Various attempts to overcome this were undertaken to prevent direct exposure of the electrolyte surface to ambient by formation of thin

Table 1. Literature review of the *type III* potentiometric gas sensors for CO₂ detection: WE–electrolyte–sensing electrode material choices, operation temperature window, detectable concentration range, response time, and references.

CO ₂ Type III Sensor Material Selection and Arrangement viz. WE/electrolyte/sensing electrode	Operating temperature [°C]	Concentration range [ppm] of CO ₂	Approx. response time [s] to CO ₂	Reference
NASICON				
Au, O ₂ NASICON Na ₂ CO ₃ CO ₂ , O ₂ , Au	320–550	10–4.7 × 10 ⁴	300	[69]
Pt, O ₂ NASICON Na ₂ CO ₃ CO ₂ , O ₂ , Pt	370–520	100–10 ⁴	120	[75]
Au, Na _{0.9} CoO _{2-y} NASICON Na ₂ CO ₃ CO ₂ , air, Au	500	10 ³ –8 × 10 ⁴	1–40 min	[72]
Au–Pd, O ₂ NASICON Na ₂ CO ₃ –BaCO ₃ CO ₂ , air, Pt	600–700	250–10 ⁴	>60	[22]
Au Na ₃ Ti ₆ O ₁₃ NASICON Na ₂ CO ₃ –BaCO ₃ CO ₂ , air, Au	500	300–50 000	<60	[70]
Pt, air NASICON Na ₃ PO ₄ –NaHCO ₃ –Na ₂ CO ₃ CO ₂ , air, Au	30	300–3000	300	[24]
Pt Na ₂ Ti ₆ O ₁₃ –Na ₂ Ti ₃ O ₇ (TiO ₂) NASICON Li ₂ CO ₃ –BaCO ₃ CO ₂ , air, Pt	500–600	500–8000	< 600	[71]
Pt NASICON Li ₂ CO ₃ –BaCO ₃ CO ₂ , air, Pt	500	300–750	63	[76]
Pt NASICON Li ₂ CO ₃ –BaCO ₃ CO ₂ , air, Au	350–550	300–2000	90–240	[25]
Pt NASICON LaCoO ₃ CO ₂ , air	200–300	100–2000	60–120	[23]
Au, BiCuVO ₄ NASICON Li ₂ CO ₃ –BaCO ₃ CO ₂ , air	400–450	100–400	180	[73]
C/Pt NASICON Na ₂ CO ₃ CO ₂ , air, Pt	465	2–10 000	60	[21]
Pt NASICON Li ₂ CO ₃ –BaCO ₃ CO ₂ , air, Pt	470	1000–10 000	12	[77]
Li₃PO₄				
Au Li ₂ TiO ₃ –TiO ₂ Li ₃ PO ₄ Li ₂ CO ₃ –BaCO ₃ CO ₂ , air, Au	450–500	500–5000	20–27	[37]
Au, Li ₂ TiO ₃ Li ₃ PO ₄ Li ₂ CO ₃ CO ₂ , air, Au	400–500	500–5000	<60	[38]
Au Li ₂ TiO ₃ Li ₃ PO ₄ Li ₂ CO ₃ CO ₂ , air, Au	350–500	16–5000	>60	[40]
Au Li ₂ TiO ₃ –TiO ₂ Li ₃ PO ₄ CO ₂ , air, Au	420–530	250–5000	>60	[39]
Au, Li ₂ TiO ₃ –TiO ₂ Li ₃ PO ₄ Li ₂ CO ₃ , air, Au	460–500	250–4000	300	[41]
Au Li ₃ PO ₄ Li ₂ CO ₃ , air, Au	500	250–2500	20	[42]
Other Li-conducting electrolytes				
Au LiCoO ₂ + 5 mol% Co ₃ O ₄ Li _{2.88} PO _{3.73} N _{0.14} Li ₂ CO ₃ CO ₂ , air, Au	400–500	200–3000	20	[44]
Pt, CO ₂ (p _o), air LISICON Li ₂ CO ₃ CO ₂ , air, Pt	500	10 ³ –10 ⁵	300	[78]
ITO, air LISICON ITO–Li ₂ CO ₃ –BaCO ₃ CO ₂ , air	30	400–2500	120	[74]
Li ₂ TiO ₃ –TiO ₂ Li _{0.35} La _{0.55} TiO ₃ Li ₂ CO ₃ CO ₂ , air, Au	300–475	500–4000	60	[51]
Au Li _{0.36} WO ₃ Li ₆ BaLa ₂ Ta ₂ O ₁₂ Li ₂ CO ₃ CO ₂ , air, Au	450–500	10–10 ⁵	>60	[53]
Au Li _{6.75} La ₃ Zr _{1.75} Ta _{0.25} O _{12-d} Li ₂ CO ₃ CO ₂ , air, Au	280–320	400–4000	<60 s	This work

layer of Al^[63] or Al₂O₃.^[64] Now, what may be unfavorable for a solid-state battery may on the other hand be of benefit for a new generation of CO₂ sensors based on Li-garnets which we propose through this work. In this case, the reaction with detected CO₂ species occurs only on the TPBs located on the surface of the electrolyte and can actively be used to monitor carbon dioxide concentration changes. In addition, one may benefit from the relatively high Li-conductivity of Li₇La₃Zr₂O₁₂ to improve the sensing response time and lower the operation temperature when compared with state-of-the-art NASICON-based CO₂ sensing devices. However, CO₂ sensor trackers based on Li₇La₃Zr₂O₁₂ garnets still do not exist, require novel electrochemical cell design and principles of operation are to be proven and explored.

In this work, we design and explore the electrochemistry of Li₇La₃Zr₂O₁₂-garnet-based materials in the scope of CO₂

sensing. For this, we employ a Ta-doped lithium lanthanum zirconate, Li_{6.75}La₃Zr_{1.75}Ta_{0.25}O_{12-δ}, with a gold RE and a mixture of Au–Li₂CO₃ as an auxiliary phase and investigate the sensing capabilities toward CO₂. Through study of the electrochemical characteristics (e.g., EMF, sensitivity per decade) and optimal operation window in terms of phase stability (e.g., bulk vs interfaces of the sensing cell) performances are evaluated. We unequivocally demonstrate by the fast sensor response time in a range of 60 s at 300 °C that Li–La–Zr-garnets are interesting electrolyte materials for future CO₂ sensor architectures as they outperform NASICON, being the current state-of-technology, operating on lower energy footprint giving new perspectives for new integrated systems of the future.

We design and fabricate potentiometric gas sensors supported on Li₇La₃Zr₂O₁₂-based solid electrolytes to investigate the applicational potential of the new materials and

materials combination toward detection of atmospheric carbon dioxide concentration changes (Figure 2a,b). Fabricated cells consist of Au RE and the working electrode (WE) being a mixture of Au and Li_2CO_3 , both brush-painted on the same face of a dense pellet of $\text{Li}_{6.75}\text{La}_3\text{Zr}_{1.75}\text{Ta}_{0.25}\text{O}_{12-\delta}$ solid electrolyte. Figure 2c shows the SEM image of the surface of as prepared RE consist of spherical Au particles of ≈ 300 nm in diameter. Figure 2d shows SEM image of the surface of the WE being a mixture of Au and Li_2CO_3 which was conditioned at 720°C to develop good interfacial contact with the solid electrolyte. We confirm that Au particles are covered with a porous layer of lithium carbonate, which is a prerequisite to engineer TPBs

for the electrochemical reaction with to-be-tracked atmospheric CO_2 . We confirm the chemical composition of the WE and stabilization of Li_2CO_3 through Raman spectroscopy. Observed Raman spectra, shown in Section S1 in the Supporting Information, consist of four sharp vibrational modes below 200 cm^{-1} and strong vibrational mode at $\approx 1098\text{ cm}^{-1}$, being a characteristic band of the C—O—C stretching mode.^[65]

Now, we turn on the phase composition and structural stability of the electrolyte by means of X-ray diffraction (XRD) and Raman spectroscopy. Since *type III* sensors are generally operated at temperatures above 400°C we probe phase stability of the electrolyte material up to expected working temperature of the device being

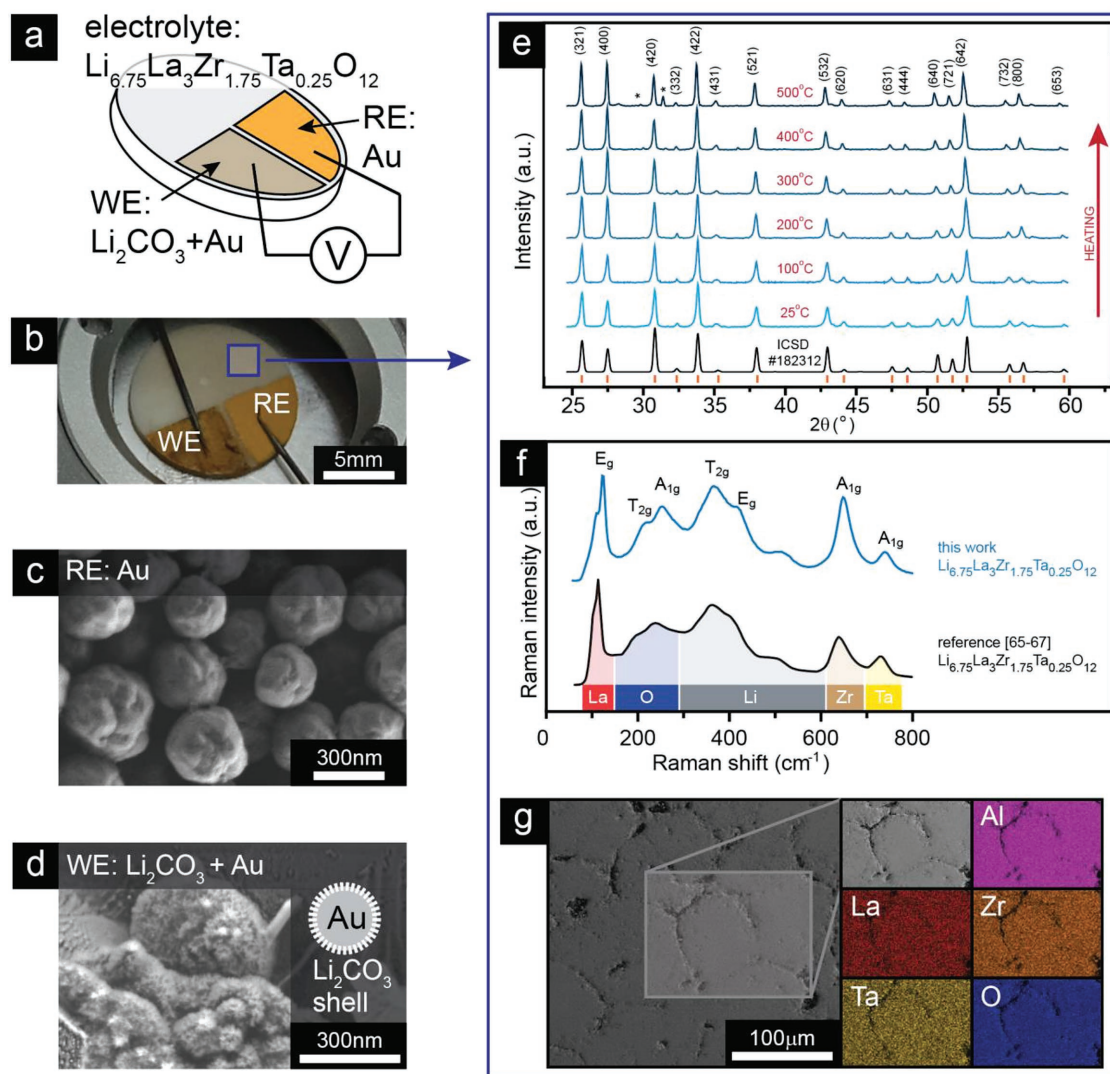


Figure 2. Cells structure. Pellet-scale potentiometric CO_2 sensor based in a) in-plane design consist. Cell consists of Au RE, $\text{Li}_{6.75}\text{La}_3\text{Zr}_{1.75}\text{Ta}_{0.25}\text{O}_{12-\delta}$ solid electrolyte, and Li_2CO_3 -Au cermet composite sensing electrode (WE). b) Sensor cell in environmental chamber during testing contacted with tungsten needles. c) SEM image of the RE composed of Au particles via brush painting. d) SEM image of the sensing electrode composed of mixture of Au particles and Li_2CO_3 after conditioning at 720°C . Porous structure and well-developed interface between sensing electrode and solid electrolyte are essential for TPB formation. Solid electrolyte. e) XRD patterns of Ta-doped lithium lanthanum zirconate solid electrolyte. XRD pattern are confirming formation of cubic-garnet phase in the *la-3d* space group (red markers) at room temperature and its thermal evolution upon heating under dry synthetic air flow. Cubic phase is preserved up to 400°C , defining the operation window of the cell. Above 400°C de-lithiated phase of $\text{La}_2\text{Zr}_2\text{O}_7$ appears. f) Raman spectrum of as prepared $\text{Li}_{6.75}\text{La}_3\text{Zr}_{1.75}\text{Ta}_{0.25}\text{O}_{12-\delta}$ solid electrolyte (blue line). Observed vibrational modes are characteristic for cubic phase of Li-garnets.^[68] g) SEM image of the electrolyte pellet surface with elemental mapping, confirming uniform distribution of La^{3+} , Zr^{4+} , Ta^{5+} , and O^{2-} .

up to ≈ 500 °C. XRD patterns of $\text{Li}_{6.75}\text{La}_3\text{Zr}_{1.75}\text{Ta}_{0.25}\text{O}_{12-\delta}$ powder at various temperatures are shown in Figure 2e. Observed diffraction peaks have been assigned to $Ia\bar{3}d$ space group, typical for cubic phase of garnet structure.^[61] We confirm that the crystal structure of the electrolyte is stable and unchanged up to ≈ 400 °C. Above 400 °C additional diffraction peaks at 28.2° and 33° appear and remain after cooling down to the room temperature. We ascribe those diffractions to be (111) and (200) peaks of the lanthanum zirconate, $\text{La}_2\text{Zr}_2\text{O}_7$, which formation might be related to possible lithium losses occurring on the surface of the electrolyte at elevated temperatures. In order to operate $\text{Li}_7\text{La}_3\text{Zr}_2\text{O}_{12}$ -based sensors within stability regime of the electrolyte, we define a safe temperature operation window for designed gas sensors below 400 °C.

Further, we investigate the near order structure by means of Raman spectroscopy. Figure 2f shows spectra collected on the surface of the dense pellet of $\text{Li}_{6.75}\text{La}_3\text{Zr}_{1.75}\text{Ta}_{0.25}\text{O}_{12-\delta}$. Spectra reveal three characteristic regions: sharp vibrational modes below 200 cm^{-1} , broad overlapping bands between 200 and 600 cm^{-1} and intense broad bands above 600 cm^{-1} . Analyzing the spectroscopic characteristics, it can be safely concluded that the cubic phase of $\text{Li}_7\text{La}_3\text{Zr}_2\text{O}_{12}$ is stabilized with no indication of secondary phases. Given that we follow with qualitative interpretation of the vibrational modes given by Larraz et al.^[66] and Tietz et al.^[67] The low-frequency part consists of two narrow bands around 107 and 120 cm^{-1} can be assigned to T_{2g} and E_g vibration modes of heavy La cations. In the intermediate Raman shifts range, we observe broad modes of 210 and 250 cm^{-1} , which can be related to T_{2g} and A_{1g} of oxygen bending modes, as well as broad bands at ≈ 360 , 410, and 514 cm^{-1} , related to T_{2g} , or E_g modes for Li-vibrations. In high wavenumbers regime, we observe strong vibration mode at $\approx 640\text{ cm}^{-1}$ followed by less intense at $\approx 730\text{ cm}^{-1}$ originated from A_{1g} stretching modes of ZrO_6 and TaO_6 octahedrons, respectively.^[68]

Figure 2g shows SEM images of the surface of the electrolyte, revealing well-developed crystallinity with grain sizes varying from 50 to $150\text{ }\mu\text{m}$ and distinctly separated grain boundaries. Elemental mapping confirms a homogeneous distribution of La, Zr, Ta, and O atoms over the grains in the electrolyte's microstructure. In addition, Al residues, being a sintering agent and coming from alumina crucibles used for sintering process, are observed. Addition of Al^{3+} facilitates densification of a bulk body and supports cubic phase stabilization by generation of Li-vacancies resulting in improved overall Li-conductivity. Estimated Li-stoichiometry is equal to 6.15 per formula unit, fulfilling cubic phase stabilization requirement of at least 0.4 Li-vacancies per formula unit.^[60] As a consequence of effective co-doping with Ta^{5+} and Al^{3+} the electrolyte used in this work shows high Li^+ conductivity of $0.74 \times 10^{-3}\text{ S cm}^{-1}$ at room temperature. More details on electric properties of $\text{Li}_{6.75}\text{La}_3\text{Zr}_{1.75}\text{Ta}_{0.25}\text{O}_{12-\delta}$ can be found in Sections S2 and S3 in the Supporting Information.

We investigate sensitivity of Ta-doped $\text{Li}_7\text{La}_3\text{Zr}_2\text{O}_{12}$ toward carbon dioxide using an in-plane geometry of the electrochemical cell, where both, sensing and reference, electrodes are exposed to the same gas environment. Viz. to fulfill the criteria of a *type III* sensor based on new electrolyte material it is the selectivity of the electrodes toward CO_2 , which defines the

sensing. In this geometry, the EMF of the cell is proportional to a difference of the chemical potentials established at the reference and sensing electrodes, according to Equation (1).

$$\text{EMF} = -\frac{\mu(\text{Li}^+)_{\text{WE}} - \mu(\text{Li}^+)_{\text{RE}}}{F} \quad (1)$$

where EMF is electromotive force of the cell, $\mu(\text{Li}^+)_{\text{WE}}$ and $\mu(\text{Li}^+)_{\text{RE}}$ are chemical potential of Li^+ in the WE and RE, respectively, and F is Faraday constant. Through the following we investigate the structural properties of the bulk sensor constituents and their interfaces, as well as studying the EMF for the model cell of O_2 , CO_2 , (Li_2CO_3 , Au) | $\text{Li}_{6.75}\text{La}_3\text{Zr}_{1.75}\text{Ta}_{0.25}\text{O}_{12-\delta}$ | Au, O_2 .

Motivated by the suited fabrication of the new sensor cells based on Ta-doped $\text{Li}_7\text{La}_3\text{Zr}_2\text{O}_{12}$ solid electrolyte, stable microstructures, and phases, we turn to sensing and electrochemical characterization by modulating the CO_2 concentration between 0 and 4000 ppm in synthetic air. The experimental details are described in Sections S4 and S5 in the Supporting Information. Response of the EMF to applied CO_2 concentration step change and its reaction time are signature characteristics to test the functionality of the newly proposed electrolyte material to track CO_2 . As sensitivity of the device follows the Nernst equation and by this it is dependent on the temperature, we investigate cells' response at selected temperatures between 278 and 411 °C (Figure 3a). The EMF of the cell shows clear response to CO_2 concentration step changes already at as low temperatures as 278 °C and rises with increasing temperature. The EMF of the cell shows a linear trend with increasing temperature up to 366 °C (Figure 3b). Above 400 °C the EMF response deviates from the theoretical predictions and the stabilization of the EMF for each applied CO_2 concentration step does not occur within 60 min. With this we confirm stability window for $\text{Li}_{6.75}\text{La}_3\text{Zr}_{1.75}\text{Ta}_{0.25}\text{O}_{12-\delta}$ to be around 400 °C, above which temperature degradation of the solid electrolyte occurs and formation of $\text{La}_2\text{Zr}_2\text{O}_7$ leads to irreversible changes of the chemical potentials of both, working and REs.

Now, based on EMF measurements, we analyze sensitivity of the cell toward applied CO_2 changes. We find that sensitivity of the cell is close to theoretical predictions between 280 and 370 °C. Distinctively, we find that calculated sensitivity of 58.2 mV per decade at 321 °C is very close to the expected value of 58.94 mV per decade, resulting from the Nernst equation. The calculated electron number at 321 °C is equal to $n = 2.03$, which value remains in good agreement with the expected value of $n = 2$ for the chemical reaction involving exchange of two electrons. With this we conclude that the dominant reaction happening in the sensor is related to cyclic redox process – occurring in the TPB of the WE formation of Li_2CO_3 , which follows Equation (2), and occurring at the interface between the solid electrolyte and porous RE cyclic formation of lithium oxide, following Equation (3).



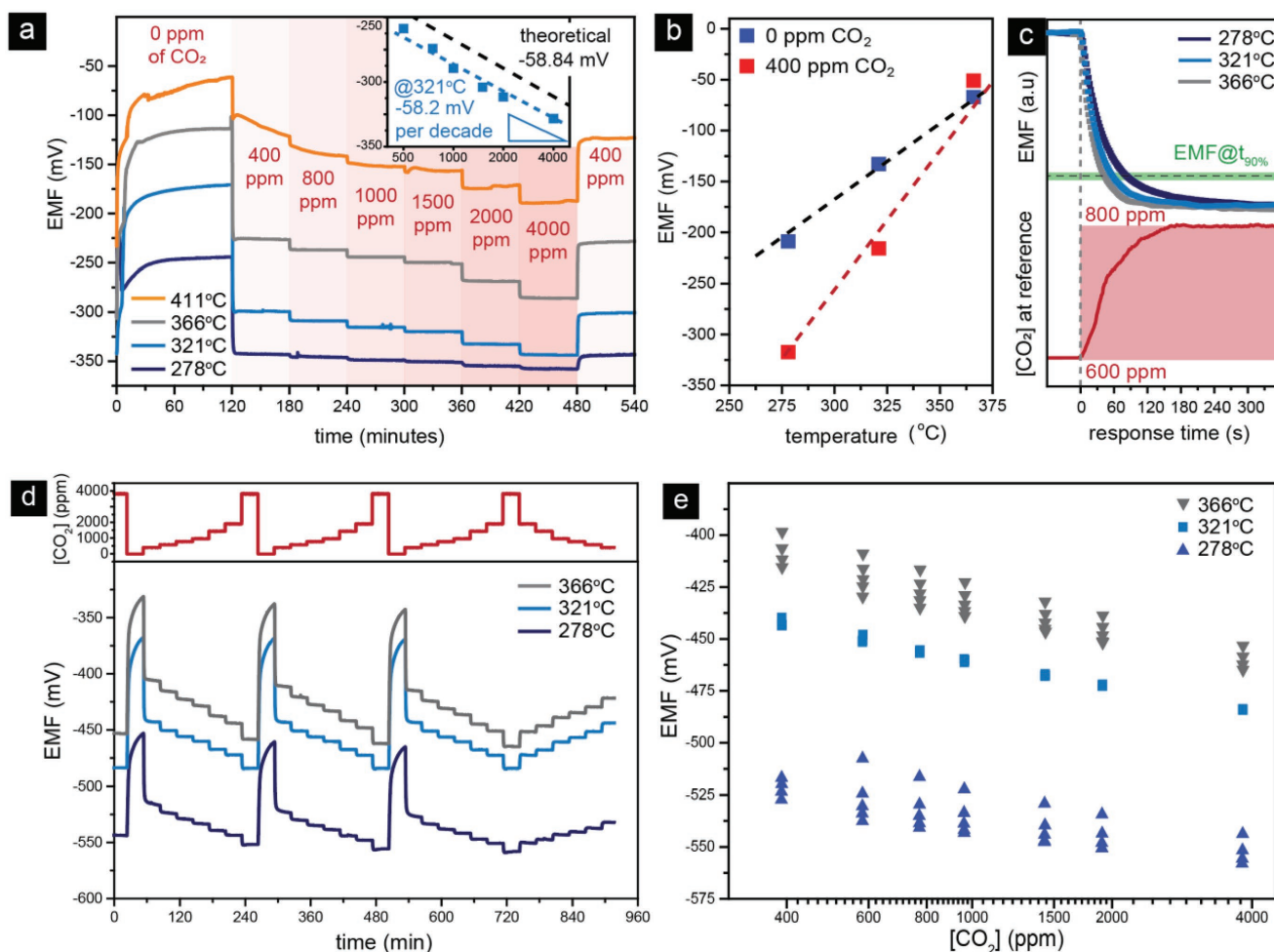


Figure 3. CO₂ sensitivity. a) EMF response to CO₂ concentration step change at selected temperatures. A clear step EMF response can be observed at temperature as low as 278 °C. The optimal sensitivity of 56.43 mV per decade, being 96% of theoretical value coming from the Nernst equation, is observed at 321 °C. b) Linear dependence of EMF as a function of temperature for selected CO₂ concentrations within temperature window for operation. c) Response time. EMF response of the cell at selected temperatures of 278 °C (navy blue), 321 °C (blue), and 366 °C (gray line) for CO₂ concentration step between 600 and 800 ppm of CO₂ detected by reference sensor (red line) as function of time. Horizontal green line shows 90% of EMF response, giving response time in a range of 60 s for 200 ppm of CO₂ step change. d) EMF changes at selected temperatures of 278 °C (navy blue line), 321 °C (blue line), and 366 °C (gray line) upon applied CO₂ step changes (red profile) collected for five consecutive CO₂ cycles at each temperature. e) EMF dependence on the CO₂ concentration in semilogarithmic scale, showing optimal stability around 321 °C.

Further, we investigate the stability of the sensing performance at selected temperatures by applying consecutive gas concentration profiles ranging from 0 to 4000 ppm of CO₂ and tracking the EMF changes over a period of few days (Figure 3d,e). The results show that we achieve ≈96% reproducibility of cell sensitivity in CO₂ range from 400 to 4000 ppm, when operated at a notably low temperature of 321 °C, which we further set as the optimum operation temperature window for the Li₇La₃Zr₂O₁₂-based CO₂ sensors. Turning to higher operation temperature at 366 °C generates a reduced sensitivity by 28%, when compared with the first cycle and is hence the upper limit of operation temperature for the given material and sensor design. To clarify the upper boundary on sensor operation and origin of reduced performance over time, we consider changes in the chemical stability of the electrolyte itself, irreversible reaction on one of the electrodes, or instability of the interface between electrolyte and the electrode.

Using Raman spectroscopy we find traces of Li₂CO₃ in the porous structure of the RE that might be causing lowered sensitivity, while the device is operated above the 400 °C. A detailed discussion of the RE stability can be found in the Supporting Information.

Finally, we look at the response times of the cells while a step change of CO₂ concentration is applied. Figure 3c shows EMF stabilization at selected temperatures during a step change of carbon dioxide concentration between 600 and 800 ppm. We observe that response time of the cell is shortened with increased temperature, due to higher reaction kinetics and resulting with 90% EMF stabilization within 60 s at 321 °C. Such a response time is rather fast among potentiometric gas sensors and is usually observed at significantly higher temperatures for devices based on other electrolytes, see Table 1. To exemplify, structurally closest to our system, Li₅La₃Nb₂O₁₂-based device shows 60 s response time around

500 °C.^[58] NASICON-based cells are showing significantly longer response times at 300 °C range which are reaching level of 60 s above 400 °C.^[69] Depending on the cell design and materials of working and REs, stabilization of the EMF requires stabilization times above 2 min. Li_3PO_4 -based cells operate in general at temperatures above 400 °C, showing rather big spread in a response time from ≈ 30 s to ≈ 5 min, depending on the system and a cell design. Other CO_2 sensing cells using such solid electrolytes as LISICON, LIPON, and $\text{Li}_{0.35}\text{La}_{0.55}\text{TiO}_3$ are usually operated at high-temperature range above 450 °C. Response times of such cells vary from ≈ 60 s up to 5 min. An exception from this trend are cells employing indium tin oxide (ITO)-composites in their WEs, which results in particularly low operating temperature of ≈ 25 °C. Authors report, however, issues with stability of those electrodes.

Placing results of our examination on the CO_2 sensitivity at low temperatures together with state-of-the-art carbon dioxide sensing devices, we demonstrate that $\text{Li}_7\text{La}_3\text{Zr}_2\text{O}_{12}$ -based sensors can be stably operated around 320 °C with fast CO_2 response time below 60 s, which is significantly lower when compared with other *type III* carbon dioxide sensors in the field (Figure 4). We bind quick response time of Li-garnet-based sensors with fast ionic exchange through the solid electrolyte–WE interface, which originates from high ionic conductivity of the electrolyte. By lowering the operation temperature window for electrochemical gas sensing, new pathways for designing cheap and energy efficient gas sensors are now accessible. The utilization of typical material for solid-state batteries in the field of CO_2 sensing gives new perspectives for electrochemical gas sensors integration with consumer electronics.

In summary, we demonstrate new type of potentiometric gas sensor based on lithium lanthanum zirconate together with electrochemistry that efficiently tracks CO_2 at relatively low temperatures leading to significantly reduced energy consumption of a device. By functionalization of $\text{Li}_{6.75}\text{La}_3\text{Zr}_{1.75}\text{Ta}_{0.25}\text{O}_{12-\delta}$

with Li_2CO_3 :Au mixture as a sensing electrode and porous layer of Au as a RE it is possible to detect CO_2 concentration changes in the atmosphere by monitoring changes of the EMF of the cell. Devices can be operated at relatively low temperatures showing close to theoretical sensitivity, good cyclability and a quick response times below 60 s already in a temperature range of 300 °C. Such fast response times are usually observed in other electrolyte material systems at high temperatures only. Obtaining quick response times at lowered operation temperature opens new perspectives for manufacturing simple sensing devices operating with low power consumption, leading to easier integration with future electronics. Presented device can monitor carbon dioxide levels up to 4000 ppm of CO_2 and beyond, being an interesting candidate for environmental and medical monitoring. To best of our knowledge, this is the first successful attempt of utilization of highly conductive cubic $\text{Li}_{6.75}\text{La}_3\text{Zr}_{1.75}\text{Ta}_{0.25}\text{O}_{12-\delta}$ solid electrolyte in electrochemical CO_2 sensing device. We conclude that it remains an interesting perspective that one can enable classic solid-state battery electrolyte materials such as Li–La–Zr-garnets to change their function from energy storage to sensing of CO_2 simply by redefining the electrode material and electrochemistry. In the Internet of Things, where sensing and power supply start to synergize, this gives room for new visions of multifunctional devices based on the similar chemistry to store energy or detect gasses, simply by the choice of electrodes and electrochemistry.

Experimental Section

Fabrication of CO_2 Pellet-Based Sensors with Li-Garnet Electrolyte—Li-Electrolyte: Solid electrolyte material, $\text{Li}_{6.75}\text{La}_3\text{Zr}_{1.75}\text{Ta}_{0.25}\text{O}_{12-\delta}$, was prepared by a solid-state reaction route to form in an initial step the nano-grained powders. A stoichiometric amount of previously dried for 24 h initial powders LiOH (Alfa Aesar, purity 99.8%), $\text{La}(\text{OH})_3$ (Sigma-Aldrich, 99.9%), ZrO_2 (Sigma-Aldrich, 99.9%), and Ta_2O_5

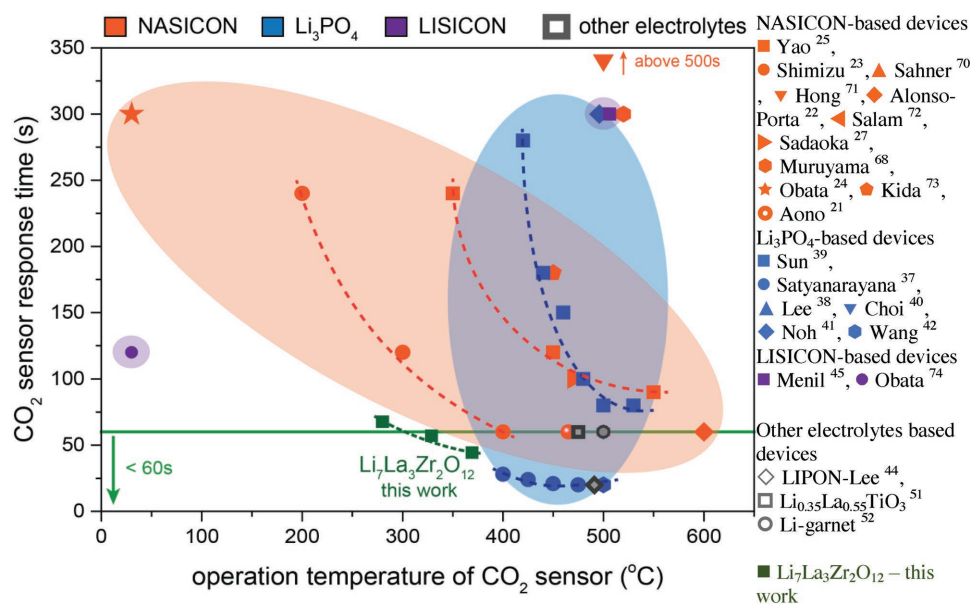


Figure 4. Comparison of the response time of CO_2 potentiometric sensors based on conventional solid electrolytes as a function of the operation temperature based on information in the literature.

(Sigma-Aldrich, 99.99%) was mixed and homogenized in a planetary ball mill in absolute isopropanol for 2 h at 400 rpm. An extra 20 mol% of LiOH was added to compensate Li-evaporation during high-temperature calcination of the powder. Al₂O₃ (Sigma-Aldrich ultra-dry, purity 99.95%) was added as a sintering agent in stoichiometric amount equal to 0.2 mol per formula. After drying in air, powder was compacted in the form of thick pellets in order to limit a high active surface area potentially prone to Li-evaporation. Synthesis was performed in alumina crucibles in a tubular furnace under constant flow of synthetic air at 850 °C for 8 h with a heating rate of 10 °C min⁻¹. Afterward pellets were crushed in a mortar, dry-grind and formed in a pellet shape of a diameter of 12 mm and thickness of 1.5 mm in a uniaxial press and then isostatically pressed with 1000 kN. Sintering of the material to a dense ceramic pellet body was held in a powder bed of the parent powder in alumina crucible under a constant flow of pure oxygen (50 sccm) at 1150 °C for 10 h with heating and cooling rates of 5 °C min⁻¹.

Electrical properties of the electrolyte material were investigated by the impedance spectroscopy with a Zahner IM6 frequency response analyzer; the applied frequency range was from 1 MHz to 100 mHz with an AC amplitude of 20 mV. Two parallel surfaces as sintered pellet of Li_{6.75}La₃Zr_{1.75}Ta_{0.25}O_{12-δ} were dry polished in Ar-filled glovebox and covered with 100 nm Au-electrodes by electron beam evaporation. The impedance measurements were performed in semi-four-probe geometry.

Fabrication of CO₂ Pellet-Based Sensors with Li-Garnet Electrolyte—Sensing and REs: The auxiliary phase was prepared from the mixture of Li₂CO₃ (Alfa Aesar, Puratronic 99.8%) and gold nanoparticles, 300–500 nm in diameter (Heraeus) in a mass ratio 5:1. The mixture of powders was homogenized in 4:1 THF:toluene in an ultrasonic bath for 60 min. The suspension was brushed directly to the surface of the pellet, dried and heated up to 725 °C in a tubular furnace under a steady flow of 1000 ppm CO₂ in dry synthetic air for 1 h with heating-cooling of 10 °C min⁻¹.

The RE was brushed on a clean surface of the electrolyte pellet from a suspension of 4:1 THF:toluene with gold particles.

Structural Characterization: The near order characterization was carried out using a confocal WiTec alpha300 M+ Raman microscope, equipped with a 532 nm laser. All Raman measurements were performed in ambient air on as-sintered pellet.

XRD patterns of the electrolyte material were recorded using Panalytical X'Pert Pro diffractometer with flat plate θ/θ geometry equipped with an X-ray tube using Ni-filtered Cu-K α radiation ($\lambda_1 = 1.54056$ Å and $\lambda_2 = 1.54439$ Å). An X'Celerator 1-D detector and a fix divergence slit (1/2°) were used. Calibration was carried out with an external LaB₆ standard. Data were collected at selected temperatures in the range ambient to 500 °C, using an AntonPaar HTK 1200 camera in a steady flow of dry synthetic air (20% O₂:80% N₂). A step size of 0.0334 and counting time of 50 s at 40 kV and 35 mA over the angular range between 25° and 60° were used for the measurements.

CO₂ Sensing Measurements: Gas sensing properties were measured in a Linkam stage of an internal volume of ≈50 cm³. The experimental setup is described in detail in Figure S3 in the Supporting Information. The sample gasses consisting of premixed dry synthetic air (21% O₂:79% N₂) and CO₂ (100% CO₂) were mixed in a set of automated mass flow controllers (MFC). The experiment consisted of two consecutive stages, in which the sensitivity of the device to CO₂ and cyclability were investigated. The temperature dependence of pCO₂ sensitivity was held with carbon dioxide steps of 0, 400, 800, 1000, 1500, 2000 and 4000 ppm of CO₂ in dry synthetic air applied for 1h each. The CO₂ profile is shown in Figure S5a in the Supporting Information. The carbon dioxide profile for investigating cyclability is presented in Figure S5b in the Supporting Information. Cyclability of the sensor was performed at calibrated temperatures of 411, 366, 321, and 278 °C with the heating/cooling rate of 10 °C min⁻¹. The temperature was monitored by type-K thermocouple during the measurements. The temperature calibration of the sensor was performed on the surface of the electrolyte pellet using Pt1000 temperature sensors glued to the surface of the electrolyte with Ag paste. The EMF of the cell was monitored with Keithley 6517B electrometer. The reference and sensing electrodes were contacted using Au covered tungsten needles.

Supporting Information

Supporting Information is available from the Wiley Online Library or from the author.

Acknowledgements

M.S., I.G., and R.P. performed and executed the experiments. J.L.M.R. discussed and supervised the work. The paper was co-written by M.S. and J.L.M.R., and all authors discussed the results and interpretations, and commented on the manuscript. The authors thank CTI Commission for Technology and Innovation for the financial support on project 17065.1 PFEN-NM and Competence Center Energy and Mobility (CCEM) and Swisselectrics for the Project 911-SLIB. J.L.M.R. thanks the Thomas Lord foundation for support of her chair and research activity at MIT.

Conflict of Interest

The authors declare no conflict of interest.

Keywords

carbon dioxide sensors, electrochemical sensors, environmental monitoring, Li-garnet, Li-ion conductors, LLZO

Received: June 27, 2018

Revised: August 8, 2018

Published online: September 20, 2018

- [1] Inventory of U.S. greenhouse gas emissions and sinks 1990–2015.
- [2] I. Joughin, B. E. Smith, B. Medley, *Science* **2014**, *344*, 735.
- [3] J. Feldmann, A. Levermann, *Proc. Natl. Acad. Sci. USA* **2015**, *112*, 14191.
- [4] E. Rignot, J. Mougino, M. Morlighem, H. Seroussi, B. Scheuchl, *Geophys. Res. Lett.* **2014**, *41*, 3502.
- [5] B. Scheuchl, J. Mougino, E. Rignot, M. Morlighem, A. Khazendar, *Geophys. Res. Lett.* **2016**, *43*, 8572.
- [6] J. M. Matter, M. Stutte, S. O. Snæbjörnsdóttir, E. H. Oelkers, S. R. Gislason, E. S. Aradóttir, B. Sigfússon, I. Gunnarson, H. Sigurdardóttir, E. Gunnlaugsson, G. Alexsson, H. A. Alfredsson, D. Wolff-Boenisch, K. Mesfin, D. F. de la Reguera Taya, J. Hall, K. Dideriksen, W. S. Broecker, *J. Mater. Sci.* **2016**, *352*, 1312.
- [7] P. Puligundla, J. Jung, S. Ko, *Food Control* **2012**, *25*, 328.
- [8] D. Zhao, D. Miller, X. Xian, F. Tsow, E. S. Forzani, *Sens. Actuators, B* **2014**, *195*, 171.
- [9] R. J. Thomas, *J. Clin. Sleep Med.* **2014**, *10*, 523.
- [10] L. Mendes, N. Ogink, N. Edouard, H. van Dooren, I. Tinoco, J. Mosquera, *Sensors* **2015**, *15*, 11239.
- [11] D. Gibson, C. MacGregor, *Sensors* **2013**, *13*, 7079.
- [12] N. Szabo, C. Lee, J. Trimboli, O. Figueroa, R. Ramamoorthy, S. Midlam-Mohler, A. Soliman, H. Verweij, P. Dutta, S. Akbar, *J. Mater. Sci.* **2013**, *38*, 4239.
- [13] T. Lang, H.-D. Wiemhoefer, W. Goepel, *Sens. Actuators, B* **1996**, *34*, 383.
- [14] W. Weppner, *Sens. Actuators* **1987**, *12*, 107.
- [15] R. Ramamoorthy, P. K. Dutta, S. A. Akbar, *J. Mater. Sci.* **2003**, *38*, 4271.
- [16] M. Kuhn, S. R. Bishop, J. L. M. Rupp, H. L. Tuller, *Acta Mater.* **2013**, *61*, 4277.
- [17] M. Gauthier, A. Chamberland, *J. Electrochem. Soc.* **1977**, *124*, 1579.
- [18] M. R. M. Jiang, M. T. Weller, *Sens. Actuators, B* **1996**, *30*, 3.

- [19] N. Imanaka, Y. Yamaguchi, G. Adachi, J. Shiokawa, *J. Electrochem. Soc.* **1986**, *133*, 1026.
- [20] Y. C. Zhang, H. Tagawa, S. Asakura, J. Mizusaki, H. Narita, *J. Electrochem. Soc.* **1997**, *144*, 4345.
- [21] H. Aono, Y. Sadaoka, L. Montanaro, E. Bartolomeo, E. Traversa, *J. Am. Ceram. Soc.* **2002**, *85*, 585.
- [22] M. Alonso-Porta, R. V. Kumar, *Sens. Actuators, B* **2000**, *71*, 173.
- [23] Y. Shimizu, N. Yamashita, *Sens. Actuators, B* **2000**, *64*, 102.
- [24] K. Obata, S. Kumazawa, K. Shimanoe, N. Miura, N. Yamazoe, *Sens. Actuators, B* **2001**, *76*, 639.
- [25] S. Yao, Y. Shimizu, N. Miura, N. Yamazoe, *Jpn. J. Appl. Phys.* **1992**, *31*, L197.
- [26] Y. Shimamoto, T. Okamoto, H. Aono, L. Montanaro, Y. Sadaoka, *Sens. Actuators, B* **2004**, *99*, 141.
- [27] Y. Sadaoka, *Sens. Actuators, B* **2007**, *121*, 194.
- [28] Y. Shimamoto, T. Okamoto, Y. Itagaki, H. Aono, Y. Sadaoka, *Sens. Actuators, B* **2004**, *99*, 113.
- [29] K. Obata, S. Matsushima, *Sens. Actuators, B* **2009**, *139*, 435.
- [30] K. Obata, S. Matsushima, *J. Ceram. Soc. Jpn.* **2010**, *118*, 213.
- [31] H. Futata, K. Ogino, *Sens. Actuators, B* **1998**, *52*, 112.
- [32] K. Kaneyasu, K. Otsuka, Y. Setoguchi, S. Sonoda, T. Nakahara, I. Aso, N. Nakagaichi, *Sens. Actuators, B* **2000**, *66*, 56.
- [33] T. Kida, K. Shimanoe, N. Miura, N. Yamazoe, *Sens. Actuators, B* **2001**, *75*, 179.
- [34] R. Izquierdo, E. Quenneville, D. Trigylidas, F. Girard, M. Meunier, D. Ivanov, M. Paleologou, A. Yelon, *J. Electrochem. Soc.* **1997**, *144*, L323.
- [35] L. Wang, R. V. Kumar, *Meas. Sci. Technol.* **2004**, *15*, 1005.
- [36] H. Narita, Z. Y. Can, J. Mizusaki, H. Tagawa, *Solid State Ionics* **1995**, *79*, 349.
- [37] L. Satyanarayana, G. Choi, W. Noh, W. Lee, J. Park, *Solid State Ionics* **2007**, *177*, 3485.
- [38] H.-K. Lee, N.-J. Choi, S. E. Moon, W. S. Yang, J. Kim, *J. Korean Phys. Soc.* **2012**, *61*, 938.
- [39] G. Sun, H. Wang, P. Li, Z. Liu, Z. Jiang, *J. Appl. Phys.* **2014**, *115*, 124505.
- [40] N.-J. Choi, H.-K. Lee, S. E. Moon, W. S. Yang, J. Kim, *Sens. Actuators, B* **2013**, *187*, 340.
- [41] W. Noh, L. Satyanarayana, J. S. Park, *Sensors* **2005**, *5*, 465.
- [42] H. Wang, D. Chen, M. Zhang, J. Wang, *Surf. Coat. Technol.* **2017**, *320*, 542.
- [43] X. Yu, J. B. Bates, F. X. Hart, *J. Electrochem. Soc.* **1997**, *144*, 524.
- [44] C. Lee, S. A. Akbar, C. O. Park, *Sens. Actuators, B* **2001**, *80*, 234.
- [45] F. Menil, B. O. Daddah, P. Tardy, H. Debeda, C. Lucat, *Sens. Actuators, B* **2005**, *107*, 695.
- [46] M. Touboul, N. Sephar, M. Quarton, *Solid State Ionics* **1990**, *38*, 225.
- [47] K. Takada, *Acta Mater.* **2013**, *61*, 759.
- [48] S. Song, J. Lu, F. Zheng, H. M. Duong, L. Lu, *RSC Adv.* **2015**, *5*, 6588.
- [49] S. Stramare, V. Thangadurai, W. Weppner, *Chem. Mater.* **2003**, *15*, 3974.
- [50] J. Z. Lee, Z. Wang, H. L. Xin, T. A. Wynn, Y. S. Meng, *J. Electrochem. Soc.* **2017**, *164*, A6268.
- [51] J. Yoon, G. Hunter, S. Akbar, P. K. Dutta, *Sens. Actuators, B* **2013**, *182*, 95.
- [52] V. Thangadurai, W. Weppner, *J. Am. Ceram. Soc.* **2005**, *88*, 411.
- [53] Y. Zhu, V. Thangadurai, W. Weppner, *Sens. Actuators, B* **2013**, *176*, 284.
- [54] J. Tan, A. Tiwari, *Electrochem. Solid-State Lett.* **2011**, *15*, A37.
- [55] Y. Jin, P. J. McGinn, *Electrochim. Acta* **2013**, *89*, 407.
- [56] J. van den Broek, S. Afyon, J. L. M. Rupp, *Adv. Energy Mater.* **2016**, *6*, 1600736.
- [57] C. Hänsel, S. Afyon, J. L. M. Rupp, *Nanoscale* **2016**, *8*, 18412.
- [58] R. Murugan, V. Thangadurai, W. Weppner, *Angew. Chem., Int. Ed.* **2007**, *46*, 7778.
- [59] C. Bernuy-Lopez, W. Manalastas, J. M. L. del Amo, A. Aguadero, F. Aguesse, J. Kilner, *Chem. Mater.* **2014**, *26*, 3610.
- [60] Y. Li, J.-T. Han, C.-A. Wang, H. Xie, J. B. Goodenough, *J. Mater. Chem.* **2012**, *22*, 15357.
- [61] H. Buschmann, J. Dolle, S. Berendts, A. Kuhn, P. Bottke, M. Wilkening, P. Heitjans, A. Senyshyn, H. Ehrenberg, A. Lotnyk, V. Duppel, L. Kienle, J. Janek, *Phys. Chem. Chem. Phys.* **2011**, *13*, 19378.
- [62] L. Cheng, E. J. Crumlin, W. Chen, R. Qiao, H. Hou, S. F. Lux, V. Zorba, R. Russo, R. Kostecki, Z. Liu, K. Persson, W. Yang, J. Cabana, T. Richardson, G. Chen, M. Doeff, *Phys. Chem. Chem. Phys.* **2014**, *16*, 18294.
- [63] C.-L. Tsai, V. Roddatis, C. V. Chandran, Q. Ma, S. Uhlenbruck, M. Bram, P. Heitjans, O. Guillon, *ACS Appl. Mater. Interfaces* **2016**, *8*, 10617.
- [64] X. Han, Y. Gong, K. Fu, X. He, G. T. Hitz, J. Dai, A. Pearse, B. Liu, H. Wang, G. Rubloff, Y. Mo, V. Thangadurai, E. Wachsman, L. Hu, *Nat. Mater.* **2016**, *16*, 572.
- [65] M. H. Brooker, J. B. Bates, *J. Chem. Phys.* **1971**, *54*, 4788.
- [66] G. Larraz, A. Orera, M. L. Sanjuán, *J. Mater. Chem. A* **2013**, *1*, 11419.
- [67] F. Tietz, T. Wegener, M. T. Gerhards, M. Giarola, G. Mariotto, *Solid State Ionics* **2013**, *230*, 77.
- [68] T. Thompson, J. Wolfenstine, J. L. Allen, M. Johannes, A. Huq, I. N. David, J. Sakamoto, *J. Mater. Chem. A* **2014**, *2*, 13431.
- [69] T. Maruyama, S. Sasaki, Y. Saito, *Solid State Ionics* **1987**, *23*, 107.
- [70] K. Sahner, A. Schulz, J. Kita, R. Merkle, J. Maier, R. Moos, *Sensors* **2008**, *8*, 4774.
- [71] H. S. Hong, J. W. Kim, S. J. Jung, C. O. Park, *Sens. Actuators, B* **2006**, *113*, 71.
- [72] F. Salam, S. Bredikhin, P. Birke, W. Weppner, *Solid State Ionics* **1998**, *110*, 319.
- [73] T. Kida, S. Kishi, M. Yuasa, K. Shimanoe, N. Yamazoe, *J. Electrochem. Soc.* **2008**, *155*, J117.
- [74] K. Obata, S. Motohi, S. Matsushima, *Sens. Mater.* **2012**, *24*, 43.
- [75] Y. Sadaoka, Y. Sakai, M. Matsumoto, T. Manabe, *J. Mater. Sci.* **1993**, *28*, 5783.
- [76] H.-Y. Dang, X.-M. Guo, *IEEE Sens. J.* **2012**, *12*, 2430.
- [77] H. J. Kim, J. W. Choi, S. D. Kim, K. S. Yoo, *Mater. Sci. Forum* **2007**, *544–545*, 925.
- [78] F. Ménil, B. O. Daddah, P. Tardy, H. Debeda, C. Lucat, *Sens. Actuators, B* **2005**, *107*, 695.